Journal of Molecular Liquids 291 (2019) 111314

Contents lists available at ScienceDirect

Journal of Molecular Liquids

journal homepage: www.elsevier.com/locate/molliq

Self-supported liquid crystal film for flexible display and photonic applications

Ramesh Manda [a], Srinivas Pagidi [a], Young Jin Lim [a], Rui He [a], Seong Min Song [a], Joong Hee Lee [a], Gi-Dong Lee [b,*], Seung Hee Lee [a,*]

[a] Applied Materials Institute for BIN Convergence, Department of BIN Convergence Technology and Department of Polymer Nano Science and Technology, Chonbuk National University, Jeonju, Jeonbuk 54896, Republic of Korea
[b] Department of Electronics Engineering, Dong-A University, Busan 49315, Republic of Korea

ARTICLE INFO

Article history:
Received 26 February 2019
Received in revised form 25 June 2019
Accepted 3 July 2019
Available online 04 July 2019

Keywords:
Flexible display
Liquid crystal
Optically isotropic phase
Kerr effect
Diffraction grating

ABSTRACT

A liquid crystal film consisted of nano-sized liquid crystal (LC) droplets <350 nm which is formed via polymerization induced phase-separation from LC/monomer composite exhibits an optically isotropic phase with mechanically self-supporting behavior. However, the film shows a slight light scattering, which deteriorates either a dark state or transparency when applied to either flexible LC displays or tunable photonic devices. Herein, we demonstrate an optically isotropic phase containing LC droplets smaller than 100 nm which exhibits a high transparency and supports bending up to 4 mm of the radius of curvature. Such nano-sized LC droplets induce strong anchoring of LC molecules at polymer interfac so that the decay response time of the device reduces to a microsecond. The paper reports the electro-optics of LC displays and diffractive properties of tunable diffractors associated with the LC droplets in detail. The bendable device demonstrated here can overcome the drawback of the conventional LC devices with non-flexibility and will have potential applications in free-form and flexible display format.

1. Introduction

Flexible display and photonic devices with fast electro-optic switching are an emerging and fast-growing technology in recent days. Liquid crystal display (LCD) exhibits strong reliability intrinsically because it is voltage driven device, however, fabricating flexible LCD requires many breakthrough technologies because bending LCD or LC photonic device deteriorates its electro-optic performance deteriorates since orientational ordering of fluid LC is disturbed by any mechanical stresses. Though, realizing the LC flexible device offers many unique properties such as lightweight, thin packing, design freedom, flexibility, and low-cost, which is a great advantage even for a futuristic technology in the wearable display and head-up displays. There have been many attempts to develop flexible LC display devices including the formation of polymer walls and networks in the inter-pixel regions [1–3], pixel isolated mode [4], fiber reinforced plastic substrate [5,6], plastic substrate [7], photo-masking [8], molding or stamping [9], active- matrix [10], and flexible photonic device [11,12]. However, the conventional LC based flexible device usually suffers from limited bending of curvature due to disturbance of the orientational ordering of LC [13]. The polymer dispersed, dichroic, and bistable cholesteric LC modes, where flexible display and photonic devices are widely explored, restrict the degree of freedom of LC molecules to flow while making stronger adhesion to the substrate overcoming some of the issues. However, the application of those LC modes was limited due to the low contrast ratio which originates from light scattering although the scattering can be utilized in smart windows. Recently, flexible displays are being more popular even in high image-quality mobile phones and the recently growing and emerging technologies like augmented reality and virtual reality which demands a fast response time <2 ms, however, the conventional LC modes are inefficient for these purposes [14,15]. Beyond the display, the LC also retains many photonic applications intended to use in many photonic devices [16]. Among those, the tunable phase gratings are well-known due to low driving operation, compact size, and non-mechanical beam steering [17]. However, the conventional LC phase grating is polarization dependent, slow response, and a limited degree of freedom to device design [18]. Although many tunable diffraction gratings are reported, they have been utilized rigid substrates. A tunable grating which is capable of steering the light beam without shape constraint is yet to be explored that could be suitable for modern flexible photonic devices.

The nano-structured LC, also known as optically isotropic LC (OILC), is a particular class of material having an outstanding behavior of sub-

* Corresponding authors.
E-mail addresses: gdlee@dau.ac.kr (G.-D. Lee), lsh1@chonbuk.ac.kr (S.H. Lee).

https://doi.org/10.1016/j.molliq.2019.111314
0167-7322/

millisecond response time and optically isotropic nature. This nano-structured LC can be a potential candidate for next-generation LC displays and tunable photonic devices because it shows wide viewing angle, cell gap insensitivity with free of surface treatment which makes the device easy processing and cost ineffective, fast response and flexibility with lightweight [19,21]. The nano-structured polymer dispersed LC (nano-PDLC) is an efficient OILC material and shows unique properties such as wider operating phase, temperature insensitive properties, and hysteresis-free [22]. Most importantly, it is a self-supported film to resist deformation against the external force which is a major requirement for flexible devices. In recent days, a variety of preparation methods and approaches of nano-PDLC has been explored and extensively studied in this regard due to less complexity in tuning the structure of the device [23–27].

The key requirement for the nano-PDLC is that the droplets of LC must be smaller than the visible wavelength, <350 nm. To meet this requirement, the nematic LC, usually, is mixed with photo-curable monomers, notably acrylate monomers, and phase-separating them through polymerization results in small LC droplets separated by thick polymer walls [28]. Here, the optically isotropic behavior was attained from the small droplets as well as the random distribution of LC directors. These LC droplets are 3-dimensionally confined in the polymer matrix that provides stronger support to the LC molecules. However, the driving mechanism of the nano-PDLC is still poorly understood. It is not possible to predict the final device properties for a given combination of LC and polymer since the device properties are relying on the LC anchoring strength at polymer walls, droplet size, and miscibility of two materials [29]. In addition, the existence of few bigger droplets in a thicker LC cell causes light leakage and this, in turn, shows a strong influence on electro-optic performances of the device with flexible substrates [3,9,30]. It has also retained a great advantage of photonic behavior because the field induced phase modulation is possible in the OILC film [31,32]. However, the conventional diffraction gratings are demonstrated on solid substrates. The flexible diffraction grating, which is suitable for use in the wearable and head-up photonic devices by providing a higher degree of freedom to overcome design contains, needs to be developed. Therefore, a more profound understanding of fundamental electro-optics of an OILC device is vital in order to yield a high-performance flexible device.

In this report, we have demonstrated a self-supported OILC film consisted of LC droplets smaller than 100 nm that exhibits a fast decay response time (134 ± 10 μs) and high transparency (~86%). This OILC film supports higher bending up to 4 mm radius of curvature without affecting the device properties. In addition, it is also capable of tuning the laser beam by the external field and act as a 1D (1-dimensional) and 2D (2-dimensional) diffraction grating. Furthermore, the electro-optics and diffractive properties are systematically studied in detail to understand the fundamental aspects of the flexible OILC device.

2. Theory

Fig. 1 shows a switching mechanism of OILC phase which consists of the LC droplets smaller than <100 nm in a continuous polymer matrix. According to Rayleigh-Gan's scattering theory, the light scattering occurs due to change in the refractive index of the medium. The fraction of scattered light (B) described as, $B = N\sigma_{avg}d$, [33]. Here, N denotes the number density of the scattering centers, σ_{avg} is the average cross-sectional area of scattering, and d is the thickness of the film at which the light is propagating. In the case of nano-PDLC, the average scattered light from the film with thickness d, is further expressed as, $\sigma_{avg} = |m\text{-}1|^2\Gamma^4R^6$, [33]. Here, R is the radius of the LC droplet, and m is the refractive index ratio of LC (n_{LC}) and polymer (n_p), Γ is a wave vector ($2\pi n_p = \lambda$), and λ is the wavelength of incident radiation. In nano-PDLC, the incident light experiences a single medium rather than two-phase medium due to the droplet size less than an incident wavelength, acting as an optically isotropic phase. When the external field is applied to this phase, the induced birefringence (Δn_{ind}) starts to generate in response to LC molecules reorientation along the field direction, known as the Kerr effect. This can be expressed as, $\Delta n_{ind} = K\lambda E^2$, where K is the Kerr constant and E is an applied electric field [34,35]. The OILC phase can be identified by the unaltered transmission on rotation of the sample under crossed polarizers, i.e., the retardation ($d\Delta n$) is zero in every direction of the incident light, Fig. 1(a). The field induced Kerr effect can be characterized by measuring the transmittance (T) resulted from reorientation of the LC in response to the field under crossed polarizers, as shown in Fig. 1(b), which can be expressed as [20],

$$T = T_o \sin^2(2\varphi) \sin^2\left(\frac{2\pi d\Delta n_{ind}(V)}{\lambda}\right) \quad (1)$$

where φ is the relative angle between the polarization direction of the incident light and the field-induced LC orientation.

3. Materials and methods

We have utilized a high dielectric anisotropy nematic LC, MLC2053 ($\Delta\varepsilon = 42.6$, $\Delta n = 0.235$ at 589.3 nm, $T_{NI} = 86$ °C, from Merck Advanced Technology in Korea), and two photo-curable monomers. Both monomers TMPTA (Trimethylolpropane Triacrylate, Sigma-Aldrich) and PETTA (Pentaerythritol Tetraacrylate, Sigma-Aldrich) are liquids at room temperature and show good miscibility with LC.

Characterization of the optically isotropic phase was performed by using the polarizing optical microscopy (POM) (Nikon eclipse, E600 POL) connected with a CCD camera (Nikon, DXM 1200). A thermally insulated hot-stage connected to a temperature controller (Instec, HSC402-STC20U) was used for the temperature controlled experiments. In order to estimate the transparency of the films, the wavelength dependent transmittance was measured with UV–Visible spectroscopy (Scinco, S-3100). The degree of phase-separation was

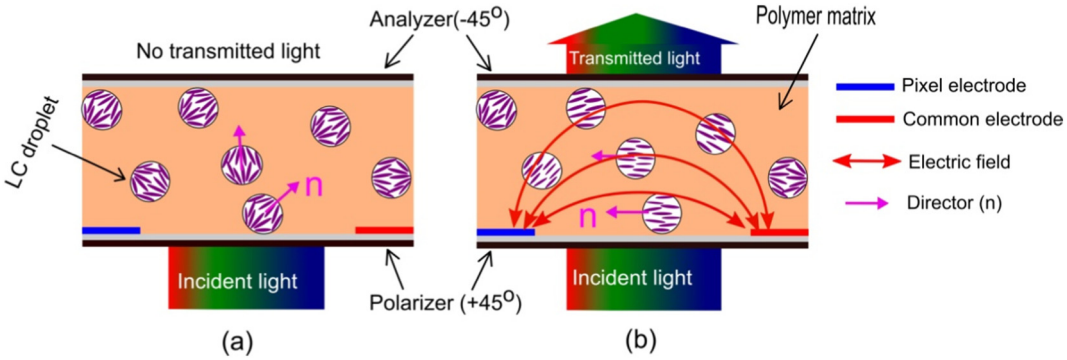

Fig. 1. Schematic of nano-PDLC at field-off state (a) and field-on state (b). The *n* represents the LC director in each droplet.

confirmed by the FTIR spectra (Shimadzu, IRTracer-100). The droplet size and polymer network scaffold are observed by using the field emission scanning electron microscope (FESEM). The in-plane switching (IPS) cell consists of comb-like interdigitated ITO (indium-tin-oxide) electrodes on the bottom substrate while no electrodes on the top substrate. Each electrode width is 4 μm, and they are separated by 4 μm providing the total active electrode area of 1.5 cm^2. No surface treatment was performed to the substrates. The separation between two substrates was maintained by the ball spacer with a diameter of 8 μm which is large enough to create half-wave retardation.

The electro-optical properties of OILC, such as voltage-dependent transmission and response time, are measured with the lab-made experimental set-up. The IPS cell is placed between crossed polarizers in such a way that the long-side IPS electrode direction makes 45° to the polarizer, and 1 kHz square-wave voltage was supplied to the cell with a function generator (Tektronix, AFG3101C) and an amplifier (FLC Electronics, A400). A He—Ne laser ($\lambda = 633$ nm) incident normal to the cell was probed and the phase response was evaluated by detecting the transmitted light with a photo-detector placed 10 cm away from the analyzer and connected to an oscilloscope (Tektronix, DPO2024B). The retardation and phase shift was measured by using REMS-150 (SESIM Photonics Technology, South Korea). The flexible and diffraction properties of this device have been demonstrated by utilizing a plastic PET (Polyethylene Terephthalate) and PI (Polyimide) substrate, respectively.

4. Results and discussions

The overall aim of this report is to prepare an efficient optically isotropic phase that enables high flexibility for LC displays and photonic devices. To do that, the thermodynamic stability of the initial mixture of the monomer and LC is essential to study in order to estimate the degree of phase-separation. Therefore, we observed the phase diagram of LC and monomer. We assume that the abrupt change in phase results from the LC and monomers only. The homogeneous mixture of LC and monomer exhibits the nematic phase (N), isotropic phase (I), and coexistence of both N and I depending on the LC ratio and temperature, as shown in Fig. 2. The number on each POM image represents the LC concentration. The POM textures of the remaining samples (below 73 wt% of LC) are similar to 73 wt% LC sample. The homogeneous mixture of LC and monomer was found to be isotropic (I) up to 73 wt% of LC concentration in the mixture. For higher LC concentration samples, above 73 wt%, the phase is initially isotropic and for time being the LC molecules are expelled from the monomer and then coalesces into bigger droplets forming nematic phase, finally resulting in a coexistence of N and I phase. The pre-cure phase-separation of LC was taken place in a continuous monomer media when the LC concentration was between 73 wt% to 95 wt%. Besides, the T_{NI} of the mixture is lowered when the monomer wt% increases over about 10%. Overall, by decreasing the LC concentration below 73 wt%, the T_{NI} of the sample was shifted toward lower temperature so that the mixture can show an optically isotropic behavior even after phase-separation between LC and monomer by UV induced polymerization.

A small amount of the radical rich photo-initiator Irgacure-907 (from Merck Advanced Technology, Korea), which shows a 365 nm excitation, was added to the above mixture to initiate the free-radical cross-linking polymerization. And then the mixture was injected into IPS cell by capillary action at isotropic temperature (above T_{NI} of NLC). The phase-separation was achieved by irradiation of UV light with 250 mW/cm^2 intensity (LC8, Lightning Cure, Hamamatsu, 365 nm emission band) for 5 min. Then the sample is cooled down to room temperature and phase-separation is performed. Here, the time duration and optimal dose of UV light are particularly important because the entire device properties depend on how efficient the phase-separation occurred. We utilized a high intensity and long curing time to optimize the polymerization which is believed to retain a stronger network

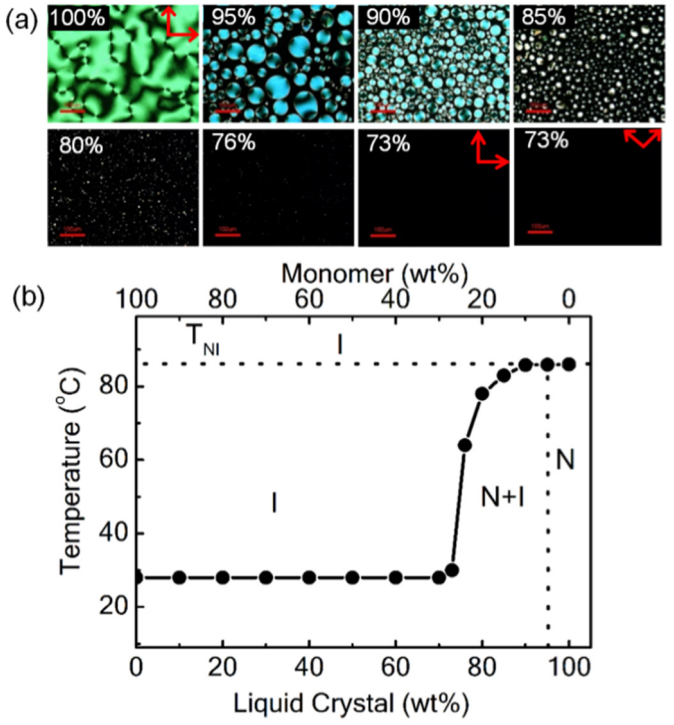

Fig. 2. (a) POM textures of the samples after several minutes of cooling below T_{NI}. The scale bar in POM images is equal to 100 μm. Red-color crossed arrows on POM images represent the polarizer and analyzer. (b) Schematic of the phase diagram measured from POM images. The horizontal dotted line represents T_{NI} of the nematic LC. N: Nematic, $N + I$: Nematic-isotropic, I: Isotropic phase. (For interpretation of the references to color in this figure legend, the reader is referred to the web version of this article.)

structure [15,22,26]. Accurate material concentrations have been shown in Table 1. In order to investigate the droplet size effect on electro-optical properties, we increase one monomer (TMPTA) concentration while keeping another monomer (PETTA) concentration is unchanged.

The FESEM measurements are performed to estimate how the smaller LC droplet was constructed in confined geometry. The characterization was done after extraction of LC from the sample by keeping the cell in Hexane for 2 days and then the two substrates are separated by a sharp-edged blade. The substrate, which has a polymer network, was coated with gold and observations made normal to the substrate, shown in Fig. 3. The filling factor of LC was calculated by measuring the droplet size by using an Image-J software, a Java-based image-processing program developed at the National Institutes of Health. The measured filling factors are 12%, 14%, 18%, 22%, and 28%, for S1, S2, S3, S4, and S5, respectively. From the droplet size distribution, it is clear that the droplets are smaller than 100 nm. On the other hand, it was also found that the majority of droplets are randomly shaped and, more importantly, the droplet size is decreasing with the increase of

Table 1
The LC and monomer concentration utilized in this report to make the nano-PDLC.

Sample	MLC2053 (wt%)	TMPTA (wt%)	PETTA (wt%)	Irgacure907 (wt%)
S0	15	54	30	1
S1	20	49	30	1
S2	25	44	30	1
S3	30	39	30	1
S4	35	34	30	1
S5	40	29	30	1

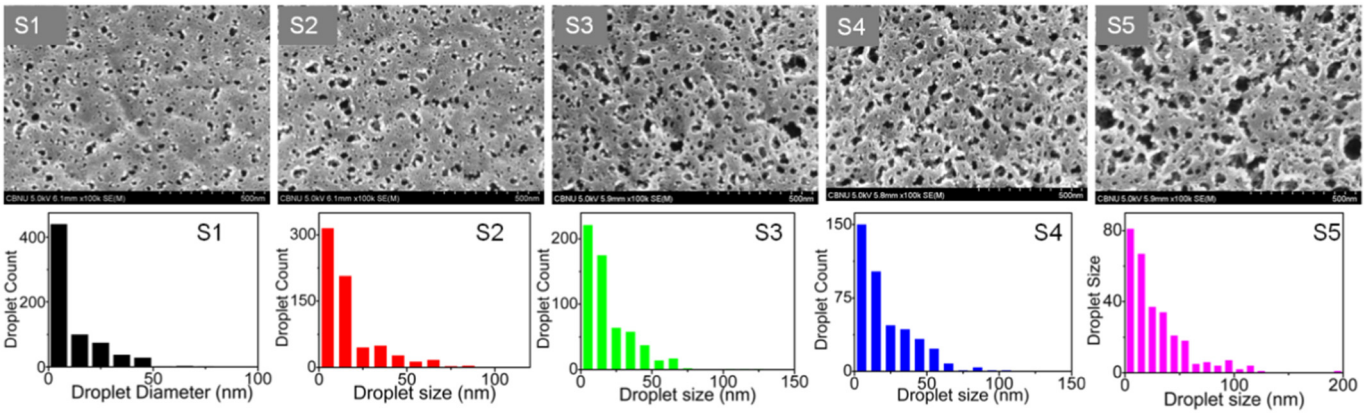

Fig. 3. The FESEM image of the polymer matrix of prepared samples (top row). The represented scale bar is 500 nm. The calculated droplet size distribution (bottom row).

monomer concentration. Another remarkable nature to notice is that many droplets are smaller than 10 nm which is, in comparison, not the similar case in conventional nano-PDLC.

The electro-optical properties such as threshold voltage (V_{th}) and operating voltage (V_{op}), which is a key operational parameter for LC device, are calculated from the voltage-dependent transmittance under crossed polarizers. The V_{th} and V_{op} are defined as the voltage required for 10% and 90% transmittance of peak transmittance, respectively. The voltage-dependent transmittance of the prepared samples is shown in Fig. 4(a). The achieved V_{th} is 25.9, 25.2, 24.5, 21.5, and 17.2 V whereas the V_{op} is 77.9, 69.2, 60.4, 51.1, and 43.8 V for S1, S2, S3, S3, S4, and S5, respectively. We found that the obtained V_{th} and V_{op} are relatively higher than that of the conventional one because the LC confined in a smaller droplet experiences stronger anchoring force at polymer surface so that the LC needs stronger dielectric coupling to reorient along the field direction [29,36]. We also measured the decaying time (τ_d) and rising time (τ_r) for all the samples, as shown in Fig. 4(b). The τ_r and τ_d are defined as the time taken for 10% to 90% transmittance change when the sample is driven to its peak transmittance and transmittance change from 90% to 10% when the applied field is withdrawn, respectively. The decay response time of the nano-PLDC can be expressed as [31],

$$\tau_d = \frac{\gamma_1 R^2}{k_{eff}\pi^2} \times \frac{1}{W_s} \tag{2}$$

where γ_1 is the rotational viscosity, R is the LC droplet size, k_{eff} is an effective elastic constant of the nematic LC, and W_s is the anchoring energy. As one can expect from the Eq. (2), the τ_d is increasing from S1 to S5. The obtained LC droplets are extremely smaller in size; therefore, the LC molecule possesses a stronger interaction with polymer walls (increases W_s) which resulted in faster relaxation time. The τ_d are 134, 142, 172, 234, and 275 μs for sample S1, S2, S3, S4, and S5, respectively. The τ_r are 858, 438, 383, 332, and 328 μs for samples S1, S2, S3, S4, and S5, respectively. The reproducibility of the measurements is 10 μs. It is interesting to notice that obtained τ_d for S1 (134 μs) is faster than reported elsewhere [37].

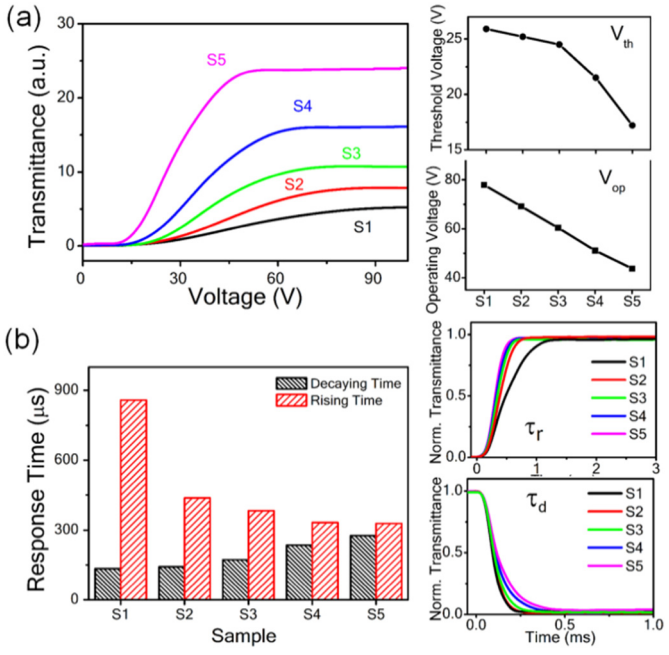

Fig. 4. (a) The voltage-dependent transmittance at 1 kHz square wave voltage. (b) The decaying and rising time of the prepared samples.

Further, the obtained OILC phase is characterized by the POM which is an essential technique to identify and characterize the optically isotropic phase. The phase appears black under crossed polarizers and no change in transmittance is observed when the sample is rotated, which is a characteristic of the OILC phase. When a field is applied, the POM image appeared bright as illustrated in Fig. 5. It is worth mentioning that the sample S0 was showing very low transmittance, indicating insufficient response to induce the birefringence. Therefore, we conclude that the minimum LC concentration required to have a proper electro-optic property is >15 wt%. However, it is highly dependent on the LC solubility in monomers and the degree of phase-separation as well. From S1 to S5, one can clearly notice that the transmittance of the dead zone, the black region between two bright strips, is reduced with increasing of LC concentration.

For a better understanding of the switching mechanism, we measured the retardation $d\Delta n_{ind}$ (V) and phase-shift $(2\pi d\Delta n_{ind}(V)/\lambda)$ of the sample, from Eq. (1), and the obtained results are presented in Fig. 6(a). Both the retardation and phase shift are increasing from S1 to S5. The maximum achieved retardation and the phase shift is 253 nm and 0.87 π, respectively, for the sample S5 at applied voltage 78 V. The relatively smaller phase-shift and retardation values are achieved from a smaller filling factor of LC. In addition, we have also measured temperature dependent Kerr constant for the sample S5 which is a key parameter to tuning performance properties of OILC. The Kerr constant was estimated from the voltage-dependent transmittance curve fit with the Kerr equation, $\Delta n_{ind} = K\lambda E^2$. As illustrated in Fig. 6(b), the measured K is mostly unaffected by the operating temperature of the sample. Unlike in the case of BPLC, whereas the K is highly dependent on the temperature of the sample, this nano-PDLC sample

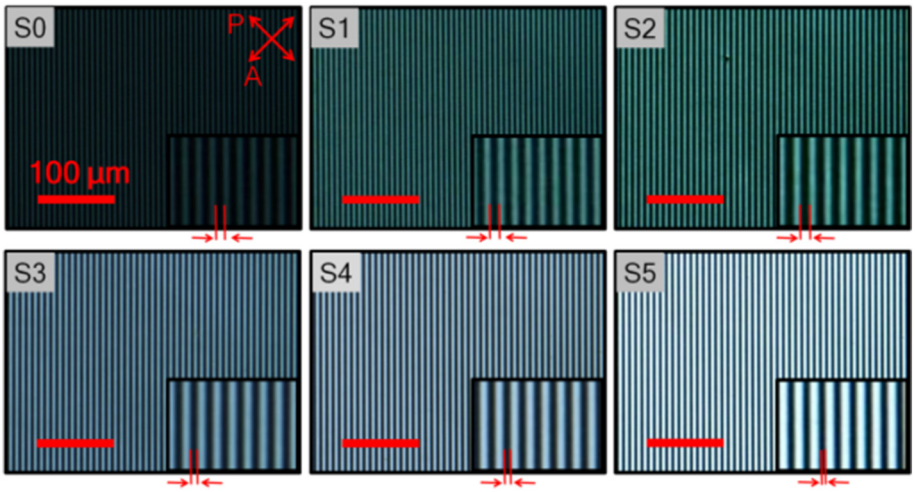

Fig. 5. The POM image of the prepared nano-PDLC samples observed at on-state. *P* and *A* indicate polarizer and analyzer, respectively. The dead-zone, the area between two bright regions, is indicated as red colored vertical lines. (For interpretation of the references to color in this figure legend, the reader is referred to the web version of this article.)

has a less sensitive on operating temperature. But the measured *K* is relatively smaller than BPLC [33,38]. Nevertheless, the *K* value is still ~200 times higher than well-known Kerr material Nitrobenzene (2.2×10^{-12} mV^{-2}) and adequate to utilize for practical applications.

For a better understanding of light scattering, we measured the transmission spectra by using a UV–Vis spectroscopy in the visible wavelength regime, shown in Fig. 7(a). Owing to the smaller LC droplets that revealed from Fig. 3, all the samples are exhibiting relatively higher transmittance, ~86%, in the visible regime that is closely matching with an empty cell. However, there is a slight transmittance deviation between OILC samples and polymerized monomers in the near-UV region. When the monomers are polymerized, drastic changes to the structure can occur such as increased molecular weight, losing specific interactions, and increasing stiffness, thereby the light absorption was occurred up to 325 nm. In the case of the pure monomer, only slight transmittance variation was noticed after polymerization. No photo-initiator was used for pre-polymerization monomers samples. In the case of S5, it is obvious that formation of few bigger droplets in 8 μm thick cell is inevitable when the LC concentration is relatively higher, thus a slight decrease in transmittance was noticed at shorter wavelength regions. The high-resolution photographic images are also showing a similar trend, as shown in Fig. 7(b). The photographic images are taken at the ambient light condition. The experiments are performed at room temperature without any external field, and no polarizers are employed. It is clearly shows that the image under the cell is clearly appearing for all the obtained samples and the level of transparency is comparable to direct appearance of the image. The transparency of the obtained samples is higher than the conventional nano-PDLC with 48 wt% of LC.

Next, the phase-separation was confirmed by using the vibrational spectroscopy, FTIR, which is a powerful tool to study the phase-separation. The degree of phase-separation was estimated by observing phase-induced changes in the absorbance spectra of the samples recorded at 2 cm^{-1} spectral resolution. We use a single silicon substrate at which the OILC mixture is spin-coated on it and performed observations before polymerization and after 5 min of UV curing. From Fig. 7(c), there are mainly three major observations at 1451, 1612, 1633, 2934 cm^{-1}. The peaks around 1612 cm^{-1} and 1633 cm^{-1}, in which the intensity decreases after polymerization, is believed to originate from the depletion of polymerizable acrylate functional group leading to the decreasing of C═C stretching vibration bands. Meanwhile, an increase of absorption bands around 2935 cm^{-1} and 1451 cm^{-1} are observed due to the increase of -CH2- stretching and bending vibration after polymerization.

To evaluate the flexibility of the film, the experiments were carried out on the plastic PET substrate with a thickness of 120 μm. The thickness of the uniformly coated ITO layer is ~110 nm. The schematic of OILC cell fabrication with the PET substrate is illustrated in Fig. 8(a). The flexible OILC film was achieved by placing the OILC mixture on a plastic substrate and carefully attaching the top substrate followed by UV curing at room temperature with 250 mW/cm^2 intensity light for 5 min. The OILC mixture, S5, was used in this demonstration and the cell gap was maintained by spraying 20 μm ball spacer on top of the bottom substrate. The phase-separation of the OILC layer gives rise to stronger adhesion to the plastic substrate and the cell gap was unaltered once the phase separation is finished. The final film exhibits enough transparency (slightly decrease due to PET substrate), as shown in Fig. 8(b). All the photographs have been taken at ambient light and temperature

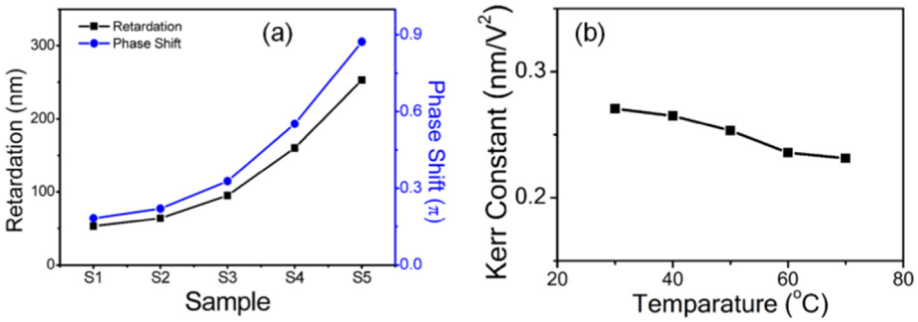

Fig. 6. (a) The measured retardation and phase shift of prepared nano-PDLC at 580 nm. (b) The temperature dependent Kerr constant of S5 (40% LC).

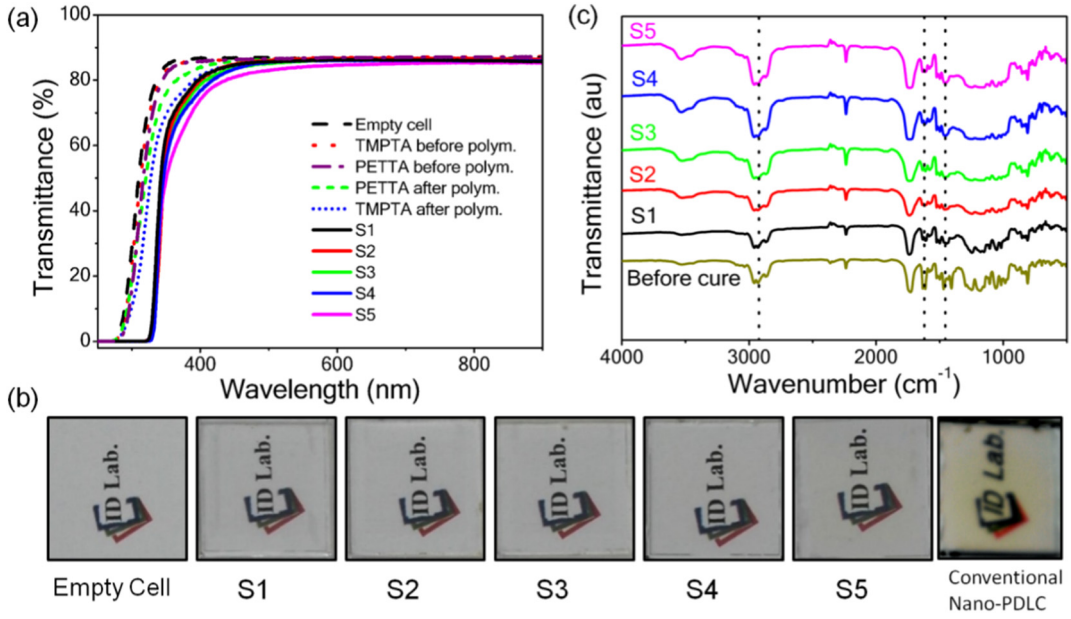

Fig. 7. (a) The transmission spectra of prepared nano-PDLC samples and (b) corresponding photographic image of the bulk cells. (c) The FTIR spectra of the nano-PDLC before phase-separation and after 5 min of UV curing of all the samples.

conditions. The film was strong enough to sustain against higher mechanical shearing forces such as cutting into pieces, Fig. 8(c). The physical damage to the film is negligible after cutting. To check the bending property, the obtained film was mechanically bent up to 8.5 mm of the radius of curvature, Fig. 8(d). Both OILC film and plastic substrates were stable and no damages were noticed on bending up to 4 mm of the radius of curvature Fig. 8(e). There was no measurable substrate detachment/delamination issue for several mechanical bending cycles (100 cycles) to the critical bending radius of 4 mm. These results reveal that the substrates are strongly attached and the film can sustain against both tensile stress and compression stress. There was no sliding of substrates effect while bending or after bending test performed to 4 mm of the radius of curvature. The dark state of the film, measured by the POM, was mostly unaltered before and after bending, Fig. 8(f). A low value indicates an excellent dark state. The dark state is measured by using i-solution image analyzing software (*i*M Technology), where the perfect dark state is defined as zero.

The bending efficiency of the obtained OILC film was confirmed by mechanically folding the cell by keeping 2 kg weight metal bar on folded film and the obtained results have been shown in Fig. 8(g). The red

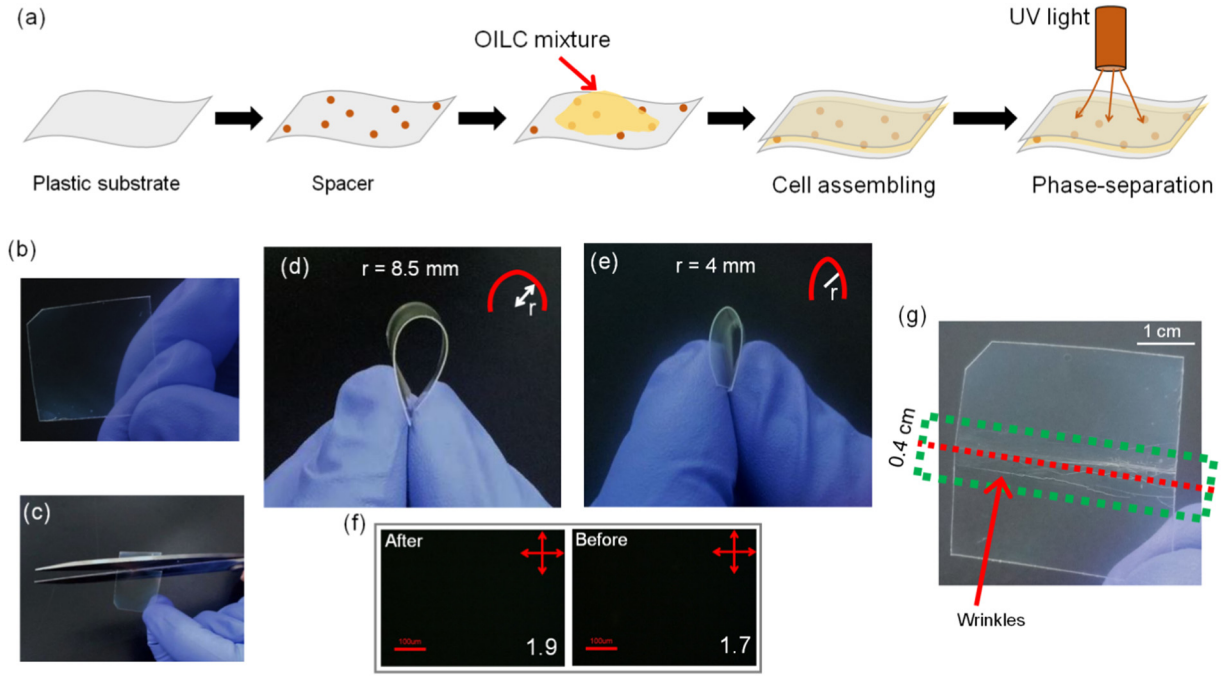

Fig. 8. (a) The schematic of preparation of flexible OILC film with PET substrate, (b) The photographic image of the final flexible film, (c) Cutting into pieces. (d) Demonstration of bending of achieved film. The *r* represents the radius of curvature of the bending film. (e) Film bending up to 4 mm of the radius of curvature. (f) POM images of the film before and after bending test. The represented scale bar is 100 μm. The number represented on the bottom of each POM image indicates an efficiency of the dark state. (g) Characterization of the folding behavior of the obtained OILC film with a flexible substrate when it is fully folded with $r = 0$ mm.

colored dotted line indicates the folding axis at which the folding was performed. The obtained results reveal that the wrinkles were generated along the folding axis on the surface of the substrate. The density of wrinkles is decreasing moving away from the folding axis covering the area ~0.4 cm wider. However, the formation of wrinkles occurs only on the substrate due to plastic deformation. We noticed that the OILC film is not much damaged even for folding, except breaking into small pieces due to plastic substrate break down. It is also showing that the two substrates are initiated to detach or delamination with OILC film after restoring back to the normal position. The delamination occurred along the folding axis. However, the OILC film is still not much damaged except breaking into smaller pieces. Moreover, there was no substrate sliding effect noticed. Considering the stronger geometrical confinement of the LC droplets by the polymer walls, there must be a less possibility of external stress influence on the LC droplets. The dense polymer network can sustain against mechanical stress imposed by the plastic substrate and tensile force induced from bending. We emphasize that the LC molecules orientation within a droplet is unaltered by the mechanical stress due to stronger geometrical confinement by the dense polymer walls. The device processing method is extremely simple and suitable for large screen fabrications. We, therefore, conclude that our approach offers an efficient way to overcome the cell gap non-uniformity and LC molecules flow issues those are the major challenges in the conventional flexible devices.

In the last step, we have characterized the diffraction properties of this flexible device at bending and non-bending positions. We have tried two different designs for the flexible diffraction grating with a single IPS substrate (1D diffractor) and double IPS substrates (2D diffractor). The PI (Polyimide) substrate consists of ITO coated IPS electrodes (ECONY, South Korea) with each electrode width and spacing is 50 μm and 20 μm, respectively. The average thickness of the PI film is 300 μm and the average thickness of patterned ITO layer is 200 nm. The bending was performed perpendicular to the grating axis, i.e., the grating vector is unaffected by bending. The schematic of diffraction measurements has been shown in Fig. 9(a). The photo-detector can be replaced by the screen appropriately to record the spatially distributed diffracted light. The He—Ne laser ($\lambda = 633$ nm) was made incident on the IPS cell at which the polarization state of the incident light directed by the polarizer's transmission axis. Here, the laser light propagates along the *x*-direction and the polarizer rotates in *yz*-plane, therefore, the polarization axis of the incident light is varying in *yz*-plane. The TM mode was chosen for measurements. The neutral density filter (*ND*) was used for minimizing the laser intensity in order to avoid unnecessary diffractions occur from patterned IPS electrodes. At field-off state, the incident light experiences isotropic refractive index (n_i) all over the sample, thus the light intensity is only focused at 0th order for a normal incident of light. When the field is applied to the grating, the incident light experiences periodic refractive index change because the LC directors inside the droplets align along the field direction generated by spatially periodic interdigitated IPS electrodes. In this case, the incident light experiences either effective ordinary (n_o) or extraordinary (n_e) refractive indices of LC director between electrode regions for TM polarization [39]. Therefore, the light passing through this phase is diffracted and the spatial collection of the diffracted light exhibits destructive and constructive interference at which the light was collected on the screen placed behind the sample. The diffraction efficiency of m^{th} order defined as,

$$\eta_m(\%) = \frac{I_m(V)}{I_o} \times 100 \tag{3}$$

where $I_m(V)$ is the light intensity of m^{th} order at the voltage V, and I_o is the intensity of the *0th* order at zero voltage. The distance between

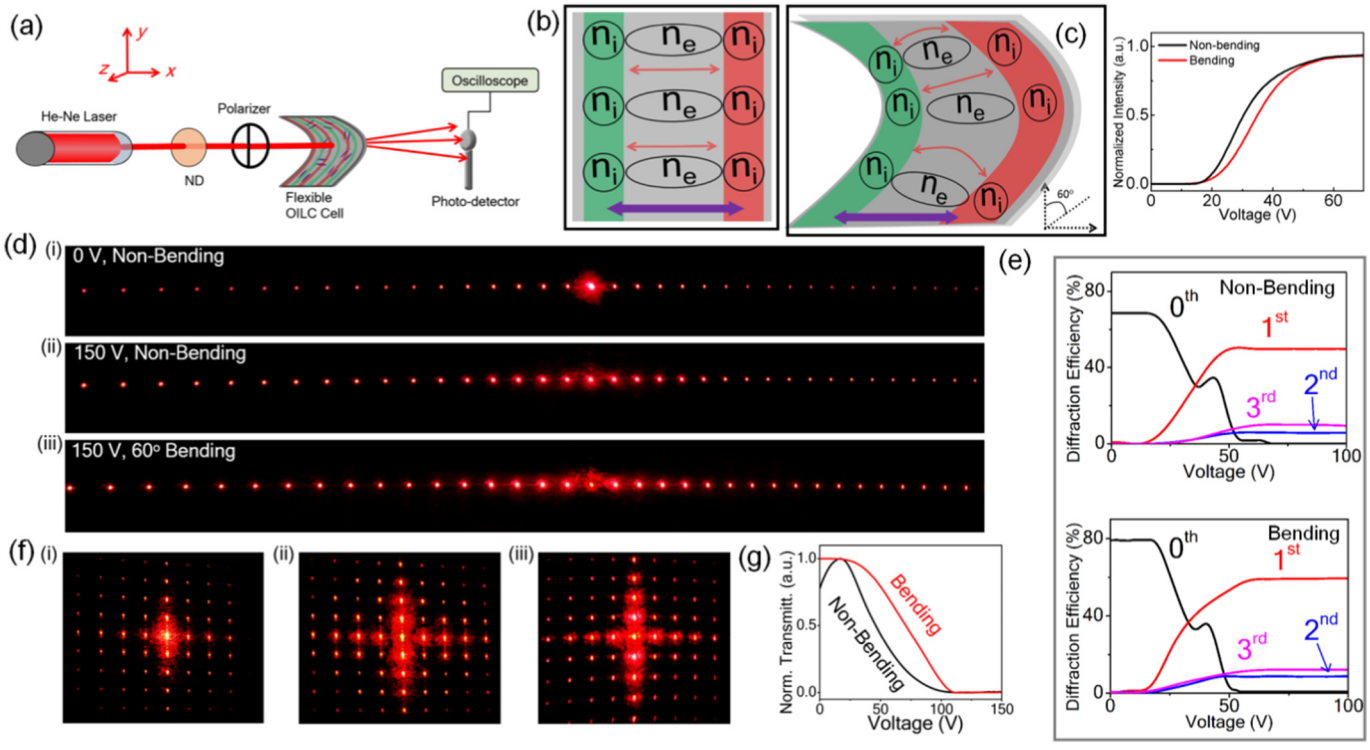

Fig. 9. (a) Schematic of diffraction efficiency measurements setup for flexible OILC film. The refractive index variation of 1D grating at, (b) non-bending and, (c) bending position. The red colored line represents electric field lines and the arrow mark (purple color) represents the polarization direction of the incident light. The voltage dependent transmittance of bending (60°) and non-bending positions under crossed polarizer's is shown in inset of (c). (d) Obtained 1D diffraction pattern at zero voltage (i), non-bending position (ii) and bending position (iii) at applied voltage. (e) The measured diffraction efficiency of 1D diffraction. (f) Obtained 2D diffraction pattern at (i) 0 V, (ii) 150 V at non-bending position, and (iii) 150 V at 10° bending position. (g) Measured 0th order intensity of 2D diffraction grating. (For interpretation of the references to color in this figure legend, the reader is referred to the web version of this article.)

screen and cell was fixed to 60 cm in order to realize a far-field approximation to form Fraunhofer diffraction.

The schematic of the refractive index change of non-bending and bending positions of 1D phase grating film is shown in Fig. 9(b) and (c), respectively. At the non-bending position, the incident light experiences the n_i at right above the electrode while incident light experiences n_e between the electrode's regions. In contrary, the refractive index of non-electrode region is expected to vary in the bending position. The stress induced by bending causes a small change in the effective refractive index of 1D grating. The V_{th} and V_{op} of the device is not much affected by bending the film up to 60°, shown in inset of Fig. 9(c), measured under crossed polarizers. From Fig. 9(d), most of the light intensity was concentrated at zero-order before applying field. After applying field, the light energy was equally distributed on either sides of the 0th order. But the energy distribution is varying from higher orders to lower orders. The spatial frequency of diffracted light is unchanged up to 60° of bending. The measured diffraction efficiency of 1D grating, defined as Eq. (3), was shown in Fig. 9(e). Interestingly, we have noticed that the diffraction efficiency is significantly improved for the film up to 60°. Even though the film supports further bending above 60°, the high sensitivity to the spatial variation of the cell leads to disturbance of diffraction pattern.

The tunable 2D diffraction grating consists of two orthogonally attached IPS substrates. From Fig. 9(f), it is clear that we achieved the 2-dimensional diffraction of an incident laser beam for both non-bending and bending positions of nano-PDLC. However, it is not supporting higher bending. In this case, we perform bending up to 10° along the bottom substrates direction. It is interesting to emphasize that the diffraction efficiency tends to increase in the bending position. The intensity profile of the 0th order is shown in Fig. 9(g). The enhanced diffraction efficiency of 0th order at 10° bending is originated from the possible increase of the effective n_e. Overall, an enormous feature of the OILC is capable to satisfy necessary properties of the next-generation photonic device. Still, the lower efficiency is the major disadvantage of this device due to lower Kerr constant. To improve the efficiency of the device, the novel techniques of polymer surface treatment such as photoalignment, are need to be adopted [40]. More researches are needed in this point of view.

5. Conclusions

We demonstrated a fast response and highly bendable optically isotropic LC film which consists of smaller than 100 nm LC droplets. This film supports the bending up to 4 mm of the radius of curvature without altering the LC orientation within the droplets. The issues associated with the conventional flexible device with the plastic substrates, like spacer detaching, fluidity of LC molecules, and the cell gap non-uniformity, have been solved by utilizing the nano-PDLC material. In addition, the obtained film is highly transparent, 86%, and exhibits an optically isotropic property in the visible wavelength regime. Furthermore, this flexible film is also promising for the fast response time, 600 μs, and act as a 1D and 2D diffractive optical element which can be integrated into the next-generation photonic devices.

Acknowledgment

This research was supported by the Basic Science Research Program (2016R1D1A1B01007189) through the National Research Foundation of Korea (NRF) funded by Ministry of Education.

References

[1] Y. Kim, J. Francl, B. Taheri, J.L. West, A method for the formation of polymer walls in liquid crystal/polymer mixtures, Appl. Phys. Lett. 72 (18) (1998) 2253–2255.
[2] H. Fujikake, T. Aida, J. Yonai, H. Kikuchi, M. Kawakita, K. Takizawa, Rigid formation of aligned polymer fiber network in ferroelectric liquid crystal, Jpn. J. Appl. Phys. 38 (9R) (1999) 5212.
[3] H. Sato, H. Fujikake, H. Kikuchi, T. Kurita, Bending tolerance of ferroelectric liquid crystal with polymer walls fastening plastic substrates, Jpn. J. Appl. Phys. 42 (5A) (2003) L476.
[4] J.W. Jung, S.K. Park, S.B. Kwon, J.H. Kim, Pixel-isolated liquid crystal mode for flexible display applications, Jpn. J. Appl. Phys. 43 (7R) (2004) 4269.
[5] W.Y. Li, P.H. Chiu, T.H. Huang, J.K. Lu, Y.H. Lai, Y.S. Huang, C.T. Chuang, C.N. Yeh, N. Sugiura, The first flexible liquid crystal display applied for wearable smart device, SID Symp. Dig. Tech. Papers 46 (1) (2015) 98–101.
[6] I.C. Kim, T.H. Kim, S.H. Lee, B.S. Kim, Extremely foldable and highly transparent nanofiber-based electrodes for liquid crystal smart devices, Sci. Rep. 8 (1) (2018) 11517.
[7] W. Lee, M. Hong, T. Hwang, S. Kim, W.S. Hong, S.U. Lee, H.I. Jeon, S.I. Kim, S.J. Baek, M. Kim, I. Nikulin, K. Chung, Transmissive 7 VGA a-Si TFT plastic LCD using low temperature process and holding spacer, SID Symp. Dig. Tech. Papers 37 (1) (2006) 1362–1364.
[8] T. Ishinabe, H. Sakai, H. Fujikake, High contrast flexible blue phase lcd with polymer walls, SID Symposium Digest of Technical Paper, vol. 46 (1), 2015, pp. 553–556.
[9] Y.T. Kim, J.H. Hong, S.D. Lee, Fabrication of a highly bendable LCD with an elastomer substrate by using a replica-molding method, J. Soc. Inf. Disp. 14 (12) (2006) 1091–1095.
[10] J. Jang, Displays develop a new flexibility, Mater. Today 9 (4) (2006) 46–52.
[11] C.C. Li, C.W. Chen, C.K. Yu, H.C. Jau, J.A. Lv, X. Qing, C.F. Lin, C.Y. Cheng, C.Y. Wang, J. Wei, Y. Yu, Arbitrary beam steering enabled by photomechanically bendable cholesteric liquid crystal polymers, Adv. Opt. Mater. 5 (4) (2017) 1600824.
[12] J. Duan, Q. Zhu, K. Qian, H. Guo, B. Zhang, Method for measurement of multi-degrees-of-freedom motion parameters based on polydimethylsiloxane cross-coupling diffraction gratings, Nanoscale Res. Lett. 12 (1) (2017) 515.
[13] S. Liu, Y. Li, P. Zhou, Q. Chen, Y. Su, Reverse-mode PSLC multi-plane optical see-through display for AR applications, Opt. Express 26 (3) (2018) 3394–3403.
[14] Y.J. Wang, P.J. Chen, X. Liang, Y.H. Lin, Augmented reality with image registration, vision correction and sunlight readability via liquid crystal devices, Sci. Rep. 7 (1) (2017) 433.
[15] R. Manda, S. Pagidi, S.S. Bhattacharyya, C.H. Park, Y.J. Lim, J.S. Gwag, S.H. Lee, Fast response and transparent optically isotropic liquid crystal diffraction grating, Opt. Express 25 (20) (2017) 24033–24043.
[16] K. Hirabayashi, T. Yamamoto, M. Yamaguchi, Free-space optical interconnections with liquid-crystal microprism arrays, Appl. Opt. 34 (14) (1995) 2571–2580.
[17] Z.G. Zheng, Y. Li, H.K. Bisoyi, L. Wang, T.J. Bunning, Q. Li, Three-dimensional control of the helical axis of a chiral nematic liquid crystal by light, Nature 531 (7594) (2016) 352.
[18] R.S. Zola, H.K. Bisoyi, H. Wang, A.M. Urbas, T.J. Bunning, Q. Li, Dynamic control of light direction enabled by stimuli-responsive liquid crystal gratings, Adv. Mater. 31 (7) (2019) 1806172.
[19] S. Matsumoto, M. Houlbert, T. Hayashi, K.I. Kubodera, Fine droplets of liquid crystals in a transparent polymer and their response to an electric field, Appl. Phys. Lett. 69 (8) (1996) 1044–1046.
[20] S.G. Kang, J.H. Kim, Optically-isotropic nanoencapsulated liquid crystal displays based on Kerr effect, Opt. Express 21 (13) (2013) 15719–15727.
[21] M.S. Kim, Y.J. Lim, S. Yoon, M.K. Kim, P. Kumar, S.W. Kang, W.S. Kang, G.D. Lee, S.H. Lee, Luminance controlled viewing angle-switchable liquid crystal display using optically isotropic liquid crystal layer, Liq. Cryst. 38 (3) (2011) 371–376.
[22] N.H. Park, S.C. Noh, P. Nayek, M.H. Lee, M.S. Kim, L.C. Chien, J.H. Lee, B.K. Kim, S.H. Lee, Optically isotropic liquid crystal mixtures and their application to high-performance liquid crystal devices, Liq. Cryst. 42 (4) (2015) 530–536.
[23] S. Aya, K.V. Le, F. Araoka, K. Ishikawa, H. Takezoe, Nanosize-induced optically isotropic nematic phase, Jpn. J. Appl. Phys. 50 (5R) (2011), 051703.
[24] S. Matsumoto, Y. Sugiyama, S. Sakata, T. Hayashi, Light processing and optical devices using nano-sized droplets of liquid crystal dispersed in polymer, J. Intell. Mater. Syst. Struct. 10 (6) (1999) 489–492.
[25] S.W. Choi, S.I. Yamamoto, Y. Haseba, H. Higuchi, H. Kikuchi, Optically isotropic nanostructured liquid crystal composite with high Kerr constant, Appl. Phys. Lett. 92 (4) (2008), 043119.
[26] N.H. Cho, P. Nayek, J.J. Lee, Y.J. Lim, J.H. Lee, S.H. Lee, H.S. Park, H.J. Lee, H.S. Kim, High-performance, in-plane switching liquid crystal device utilizing an optically isotropic liquid crystal blend of nanostructured liquid crystal droplets in a polymer matrix, Mater. Lett. 153 (2015) 136–139.
[27] N. Kim, D.Y. Kim, M. Park, Y.J. Choi, S. Kim, S.H. Lee, K.U. Jeong, Optically isotropic liquid crystal media formulated by doping star-shaped cyclicoligosiloxane liquid crystal surfactants in twin nematic liquid crystals, Soft Matter 11 (19) (2015) 3772–3779.
[28] J.L. West, Phase separation of liquid crystals in polymers, Mol. Cryst. Liq. Cryst. 157 (1) (1988) 427–441.
[29] Y.J. Lim, J.H. Yoon, H. Yoo, S.M. Song, R. Manda, S. Pagidi, M.H. Lee, J.M. Myoung, S.H. Lee, Fast switchable field-induced optical birefringence in highly transparent polymer-liquid crystal composite, Opt. Mater. Express 8 (12) (2018) 3698–3707.
[30] S.M. Ji, J.W. Huh, J.H. Kim, Y. Choi, B.H. Yu, T.H. Yoon, Fabrication of flexible light shutter using liquid crystals with polymer structure, Liq. Cryst. 44 (9) (2017) 1429–1435.
[31] L. Rao, Z. Ge, S. Gauza, K.M. Chen, S.T. Wu, Emerging liquid crystal displays based on the Kerr effect, Mol. Cryst. Liq. Cryst. 527 (1) (2010) 30–186.

[32] R. Manda, S. Pagidi, S.S. Bhattacharya, H. Yoo, A. Kumar, Y.J. Lim, S.H. Lee, Ultrafast switching blue phase liquid crystals diffraction grating stabilized by chiral monomer, J. Phys. D. Appl. Phys. 51 (18) (2018), 185103.
[33] S. Zumer, J. Doane, Light scattering from a small nematic droplet, Phys. Rev. A 34 (4) (1986) 3373–3386.
[34] J. Kerr, Xl. A new relation between electricity and light: dielectrified media birefringent, London Edinburgh Dublin Phil. Mag. J. Sci. 50 (332) (1875) 337–348.
[35] R. Yamamoto, S. Ishihara, S. Hayakawa, K. Morimoto, The Kerr constants and relaxation times in the isotropic phase of nematic homologous series, Phys. Lett. A 69 (4) (1978) 276–278.
[36] S. Pagidi, R. Manda, Y.J. Lim, S.M. Song, H. Yoo, J.H. Woo, Y.H. Lin, S.H. Lee, Helical pitch dependent electro-optics of optically high transparent nano-phase separated liquid crystals, Opt. Express 26 (21) (2018) 27368–27380.
[37] B. Kim, H.G. Kim, G.Y. Shim, J.S. Park, K.I. Joo, D.J. Lee, J.H. Lee, J.H. Baek, B.K. Kim, Y. Choi, H.R. Kim, Fast-switching optically isotropic liquid crystal nano-droplets with improved depolarization and Kerr effect by doping high k nanoparticles, Appl. Opt. 57 (2) (2018) 119–129.
[38] J. Li, W. Du, A. Gao, G. Bie, M. Hu, H. Chen, S.T. Wu, Enlarging the Kerr constant of polymer-stabilised blue phases with a novel chiral monomer, Liq. Cryst. 43 (7) (2016) 937–943.
[39] Y. Hori, K. Asai, M. Fukai, Field-controllable liquid-crystal phase grating, IEEE Trans. Electron Devices 26 (11) (1979) 1734–1737.
[40] V.G. Chigrinov, V.M. Kozenkov, H.S. Kwok, Photoalignment of Liquid Crystalline Materials: Physics and Applications, vol. 17, John Wiley & Sons, 2008.